Outer Sphere Metal-to-Ligand Charge Transfer in Organometallic Ion Pairs

Lucian A. Lucia, Khalil Abboud, and Kirk S. Schanze*

Department of Chemistry, University of Florida, Gainesville, Florida 32611-7200

Received March 27, 1997[⊗]

A series of organometallic salts which comprise a *fac*-(b)$Re^{I}(CO)_3(py)^+$ cation (b = 4,4′,5,5′-tetramethyl-2,2′-bipyridine (tmb), 2,2′-bipyridine (bpy), or 4,4′-dicarbomethoxy-2,2′-bipyridine (dmeb); py = pyridine) paired with the $Co(CO)_4^-$ anion have been prepared and subjected to photophysical study. In nonpolar solvents the salts feature a broad, low-intensity ion-pair charge transfer (IPCT) absorption band. The energy of the IPCT band decreases with the LUMO energy of the diimine ligand, suggesting that the orbital basis of the transition is d (Co) → π^* (b). An X-ray crystal structure of [(bpy)$Re^{I}(CO)_3(py)^+$][$Co(CO)_4^-$] (**2a**) reveals that the anion occupies a lattice position which is directly below (or above) the plane defined by the bpy ligand, which supports the d (Co) → π^* (b) IPCT assignment. Luminescence studies of the salts indicate that the dπ (Re) → π^* (b) metal-to-ligand charge transfer (MLCT) excited state is quenched by reductive electron transfer from $Co(CO)_4^-$. Nominally IPCT and MLCT excitation of the organometallic ion pairs afford the same geminate radical pair, [($b^{\bullet-}$)$Re^{I}(CO)_3(py)$,$Co(CO)_4^{\bullet}$]. However, laser flash photolysis studies reveal that the rate of charge recombination within the geminate radical pair is significantly slower when MLCT excitation is applied. The slower rate of charge recombination is attributed to the fact that triplet state geminate pairs are produced via the triplet MLCT excited state manifold.

Introduction

Bimolecular photoinduced electron transfer between donors and acceptors in fluid solution leads to production of ion radicals (or neutral radicals) with varying degrees of efficiency. Detailed studies of the efficiency for charge separation in organic donor−acceptor pairs has led to a thorough understanding of the structure of geminate radical (ion) pairs and the dynamics of highly exothermic electron transfer within them.[1−36] Organic donor−acceptor systems feature a number of properties that facilitate studies of bimolecular photoinduced electron transfer, namely, high radiative rates for fluorescence from the locally excited (LE) states of the photoexcited acceptor (or donor),[37] as well as exciplex fluorescence[2,14,15] and/or Mulliken electron donor−acceptor (EDA) complex formation.[38] By taking advantage of these unique properties, several research groups developed concise models which elucidate the factors that control competition between charge recombination, exciplex formation, and free radical (ion) formation in organic systems.[3−36]

Bimolecular photoinduced electron transfer reactions involving a transition metal ion as the donor and/or acceptor have also been examined in great detail.[39−47] A particular focus in

* Corresponding author. E-mail: kschanze@chem.ufl.edu.

⊗ Abstract published in *Advance ACS Abstracts,* December 1, 1997.

(1) For an excellent overview of the field of photoinduced electron transfer see: *Photoinduced Electron Transfer*, Fox, M. A., Chanon, M. D., Eds.; Elsevier: Amsterdam, 1988; Parts A−D.
(2) *The Exciplex*, Ware, W. R., Ed.; Academic Press: New York, 1975.
(3) Mattes, S. L.; Farid, S. *Science* **1984**, *226*, 917.
(4) Gould, I. R.; Ege, D.; Mattes, S. L.; Farid, S. *J. Am. Chem. Soc.* **1987**, *109*, 3794.
(5) Gould, I. R.; Moser, J. E.; Ege, D.; Moody, R.; Farid, S. *J. Am. Chem. Soc.* **1988**, *110*, 1991.
(6) Gould, I. R.; Moody, R.; Farid, S. *J. Am. Chem. Soc.* **1988**, *110*, 7242.
(7) Gould, I. R.; Moody, R.; Farid, S. *J. Am. Chem. Soc.* **1990**, *112*, 4290.
(8) Todd, W. P.; Dinnocenzo, J. P.; Farid, S.; Goodman, J. L.; Gould, I. R. *J. Am. Chem. Soc.* **1991**, *113*, 3601.
(9) Gould, I. R.; Young, R. H.; Moody, R. E.; Farid, S. *J. Phys. Chem.* **1991**, *95*, 2068.
(10) Gould, I. R.; Farid, S. *J. Phys. Chem.* **1992**, *96*, 7635.
(11) Gould, I. R.; Noukakis, D.; Gomez-Jahn, L.; Goodman, J. L.; Farid, S. *J. Am. Chem. Soc.* **1993**, *115*, 4405.
(12) Gould, I. R.; Noukakis, D.; Goodman, J. L.; Young, R. H.; Farid, S. *J. Am. Chem. Soc.* **1993**, *115*, 3830.
(13) Gould, I. R.; Farid, S. *J. Am. Chem. Soc.* **1993**, *115*, 4814.
(14) Gould, I. R.; Young, R. H.; Mueller, L. J.; Farid, S. *J. Am. Chem. Soc.* **1994**, *116*, 8176.
(15) Gould, I. R.; Young, R. H.; Mueller, L. J.; Albrecht, A. C.; Farid, S. *J. Am. Chem. Soc.* **1994**, *116*, 8188.
(16) Farid, S.; Gould, I. R. *J. Am. Chem. Soc.* **1995**, *117*, 4399.
(17) Miyasaka, H.; Ojima, S.; Mataga, N. *J. Phys. Chem.* **1989**, *93*, 3380.
(18) Mataga, N.; Asahi, T.; Kanda, Y.; Okada, T.; Kakitani, T. *Chem. Phys.* **1988**, *127*, 249.
(19) Asahi, T.; Mataga, N. *J. Phys. Chem.* **1989**, *93*, 6575.
(20) Mataga, N.; Nishikawa, S.; Asahi, T.; Okada, T. *J. Phys. Chem.* **1990**, *94*, 1443.
(21) Ojima, S.; Miyasaka, H.; Mataga, N. *J. Phys. Chem.* **1990**, *94*, 4147.
(22) Ojima, S.; Miyasaka, H.; Mataga, N. *J. Phys. Chem.* **1990**, *94*, 5834.
(23) Ojima, S.; Miyasaka, H.; Mataga, N. *J. Phys. Chem.* **1990**, *94*, 7534.
(24) Peters, K. S.; Lee, J. *J. Phys. Chem.* **1992**, *96*, 8941.
(25) Peters, K. S.; Lee, J. *J. Am. Chem. Soc.* **1993**, *115*, 9643.
(26) Li, B.; Peters, K. S. *J. Phys. Chem.* **1993**, *97*, 7648.
(27) Li, B.; Peters, K. S. *J. Phys. Chem.* **1993**, *97*, 13145.
(28) Peters, K. S. *Adv. Electron Transfer Chem.* **1994**, *4*, 27.
(29) Bockman, T. M.; Kochi, J. K. *J. Chem. Soc., Perkin Trans. 2* **1994**, 1901.
(30) Hubig, S. M.; Bockman, T. M.; Kochi, J. K. *J. Am. Chem. Soc.* **1996**, *118*, 3842.
(31) Bockman, T. M.; Hubig, S. M.; Kochi, J. K. *J. Am. Chem. Soc.* **1996**, *118*, 4502.
(32) Bockman, T. M.; Kochi, J. K. *J. Chem. Soc., Perkin Trans. 2* **1996**, 1633.
(33) Sankararaman, S.; Perrier, S.; Kochi, J. K. *J. Am. Chem. Soc.* **1989**, *111*, 6448.
(34) Sankararaman, S.; Kochi, J. K. *J. Chem. Soc., Chem. Commun.* **1989**, 1800.
(35) Yabe, T.; Kochi, J. K. *J. Am. Chem. Soc.* **1992**, *114*, 4491.
(36) Bockman, T. M.; Lee, K. Y.; Kochi, J. K. *J. Chem. Soc., Perkin Trans. 2* **1992**, 1581.
(37) Birks, J. B. *Photophysics of Aromatic Molecules*; Wiley-Interscience: New York, 1970.
(38) Mulliken, R. S.; Person, W. B. *Molecular Complexes*; Wiley-Interscience: New York, 1969.
(39) Bock, C. R.; Meyer, T. J.; Whitten, D. G. *J. Am. Chem. Soc.* **1974**, *96*, 4710.
(40) Bock, C. R.; Connor, J. A.; Guitierrez, A. R.; Meyer, T. J.; Whitten, D. G.; Sullivan, B. P.; Nagle, J. K. *J. Am. Chem. Soc.* **1979**, *101*, 4815.
(41) Sutin, N.; Creutz, C. *J. Chem. Educ.* **1983**, *60*, 809.
(42) Georgopoulos, M.; Hoffman, M. Z. *J. Phys. Chem.* **1991**, *95*, 7717.
(43) Sun, H.; Hoffman, M. Z. *J. Phys. Chem.* **1994**, *98*, 11719.
(44) Clark, C. D.; Hoffman, M. Z. *J. Phys. Chem.* **1996**, *100*, 14688.

S0020-1669(97)00351-0 CCC: $14.00

this case has been on systems in which a metal-to-ligand charge transfer (MLCT) excited state metal complex acts as the electron donor or acceptor. Generally, the yields of free radical (ions) resulting from bimolecular photoinduced electron transfer reactions involving MLCT states are comparatively large.[42−47] However, because radiative decay rates for MLCT states are relatively low[48,49] and exciplex emission and EDA complex formation is unusual in transition metal systems, it has been more difficult to develop a concise description of the factors that control competition between charge recombination and free radical (ion) formation in these systems.

Ion pairs formed between electron poor cations and electron rich anions feature absorption bands due to ion-pair charge transfer (IPCT) from the donor anion to the acceptor cation.[50,51] IPCT bands are observed in many systems that involve a transition metal complex.[50,51] In these systems, the IPCT transition is closely similar to the charge transfer absorption band observed in organic-based EDA complexes.[38] Specifically, IPCT excitation is believed to lead directly to a radical (ion) pair state as a result of photoinduced electron transfer from the donor anion to the acceptor cation. By analogy, excitation of an organic EDA complex also leads directly to a contact radical ion-pair state.[9,10]

Kochi and co-workers prepared salts comprised of the carbonylmetallate donors $Co(CO)_4^-$, $Mn(CO)_5^-$, and $V(CO)_6^-$ and cationic organic acceptors such as pyridinium and *N*-methylquinolinium (Q^+).[52−55] In solution the organometallic ion pairs feature broad, weak absorption bands in the mid-visible due to IPCT from the carbonylmetallate anion to the organic cation. The charge transfer assignment is supported by the fact that the energy of the optical transition for a series of acceptor cations with a given carbonylmetallate donor correlates linearly (with unit slope) with the electrochemical reduction potentials of the cations.[52] Moreover, that IPCT excitation of the organometallic ion pairs directly affords a radical pair state is demonstrated by the observation of the products of electron transfer, either by transient spectroscopy, or as permanent photochemical change.

We have an interest in bimolecular photoinduced electron transfer reactions of MLCT excited states in complexes of the type *fac*-(b)$Re^I(CO)_3(py)^+$ (where b = a diimine ligand such as 2,2′-bipyridine and py = pyridine).[47,56] The MLCT state of these complexes is quenched efficiently by neutral organic electron donors such as tertiary amines.[47] Moreover, MLCT quenching is accompanied by production of long-lived radical (ions) in comparatively high yields, which indicates that cage escape from the geminate radical (ion) pairs formed by photoinduced electron transfer competes effectively with charge recombination.[47] The rates of charge recombination that are calculated from the cage escape yields are low by comparison with rates determined for geminate radical ion pairs in organic based systems. The best explanation for this discrepency is that in the metal complex systems the geminate radical pair has triplet spin character which effectively slows down charge recombination.[46,47]

In an effort to provide further insight into the factors that control charge recombination and cage escape in transition metal complex systems, a study of ion-pair charge transfer complexes **1a**, **2a**, and **3a** was initiated. These complexes comprise a series

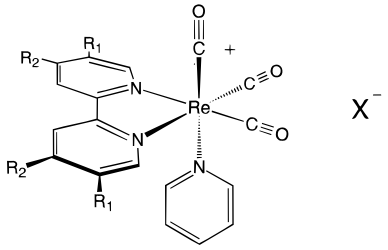

1a : R_1 = H, R_2 = CO_2Me, X^- = $Co(CO)_4^-$

1b : R_1 = H, R_2 = CO_2Me, X^- = PF_6^-

2a : R_1 = H, R_2 = H, X^- = $Co(CO)_4^-$

2b : R_1 = H, R_2 = H, X^- = PF_6^-

3a : R_1 = CH_3, R_2 = CH_3, X^- = $Co(CO)_4^-$

3b : R_1 = CH_3, R_2 = CH_3, X^- = PF_6^-

of (b)$Re^I(CO)_3(py)^+$ cations paired with the $Co(CO)_4^-$ donor and were designed to allow comparison of the cage escape efficiency for photoinduced electron transfer resulting either from MLCT excitation of the transition metal chromophore or by direct excitation of the IPCT transition of the donor−acceptor pair. Differences in cage escape efficiency were anticipated because of several factors. First, MLCT excitation is likely to produce a mixture of solvent separated and contact radical pairs;[6,9,10,19] by contrast, direct IPCT excitation exclusively affords contact radical pairs.[38,50,51] Second, MLCT excitation may produce a triplet spin-correlated geminate pair,[46,47,57] while direct IPCT excitation is likely to generate singlet geminate pairs. Thus, it was anticipated that this system would display features similar to organic systems studied earlier in which a difference in the cage escape efficiency was observed for geminate radical (ion) pairs produced by diffusional quenching of the locally excited state of an organic acceptor compared to those formed by direct excitation of a charge transfer band in the Mulliken-type EDA complexes.[6,9,10,19]

The present report describes the synthesis, structural characterization, and photophysical study of the series of salts **1a**, **2a**, and **3a**. As expected, these complexes feature a moderately intense Re → diimine MLCT absorption in the near-UV.[58] Furthermore, in nonpolar solvents the complexes display a weak, broad absorption that is assigned to IPCT from the carbonylcobaltate donor to the Re(I) acceptor. Luminescence studies indicate that the MLCT state of the Re(I) chromophore is strongly quenched, presumably via electron transfer from $Co(CO)_4^-$, and laser flash photolysis confirms the electron transfer mechanism by demonstrating the appearance of the expected transient radical products. Quantitative transient

(45) Ohno, T.; Yoshimura, A.; Mataga, N.; Tazuke, S.; Kawanishi, Y.; Kitamura, N. *J. Phys. Chem.* **1989**, *93*, 3546.
(46) Ohno, T.; Yoshimura, A.; Mataga, N. *J. Phys. Chem.* **1990**, *94*, 4817.
(47) Lucia, L. A.; Schanze, K. S. *Inorg. Chim. Acta* **1994**, *225*, 41.
(48) Caspar, J. V.; Kober, E. M.; Sullivan, B. P.; Meyer, T. J. *J. Am. Chem. Soc.* **1982**, *104*, 41.
(49) Caspar, J. V.; Meyer, T. J. *Inorg. Chem.* **1983**, *22*, 2444.
(50) Vogler, A.; Kunkely, H. In *Photoinduced Electron Transfer II*; Mattay, J., Ed.; Topics in Current Chemistry, Vol. 158; Springer-Verlag: Berlin, 1990; p 1.
(51) Billing, R.; Rehorek, D.; Henning, H. In Photoinduced Electron Transfer II; Mattay, J., Ed.; Topics in Current Chemistry, Vol. 158; Springer-Verlag: Berlin, p 151.
(52) Bockman, T. M.; Kochi, J. K. *J. Am. Chem. Soc.* **1989**, *111*, 4669.
(53) Bockman, T. M.; Kochi, J. K. *New J. Chem.* **1992**, *16*, 39.
(54) Wei, C.-H.; Bockman, T. M.; Kochi, J. K. *J. Organomet. Chem.* **1992**, *428*, 85.
(55) Kochi, J. K.; Bockman, T. M. *Adv. Organomet. Chem.* **1991**, *33*, 52.
(56) Throughout the paper the following ligand abbreviations are used: b = a diimine ligand such as 2,2′-bipyridine; tmb = 4,4′,5,5′-tetramethyl-2,2′-bipyridine, bpy = 2,2′-bipyridine, dmeb = 4,4′-dicarbomethoxy-2,2′-bipyridine.
(57) Wolff, H.-J.; Bürssner, D.; Steiner, U. E. *Pure Appl. Chem.* **1995**, *67*, 167.
(58) Wrighton, M. S.; Geoffroy, G. L. *Organometallic Photochemistry*; Academic Press: New York, 1979.

Table 1. Photophysical and Electrochemical Characteristics of Re(I) Cations[a]

complex	$E_{1/2}$(b/b$^{\bullet-}$)[b]/eV	E_{MLCT}[c]/eV	Φ_{em}	τ_{em}/ns	ΔG_{fet}[d]/eV	Φ_{ce}(355 nm)[e]	Φ_{ce}(532 nm)[f]
1b	−0.67	2.15		75	−1.15		
2b	−1.16	2.38	0.055	234	−0.89	0.65 ± 0.1	0.04 ± 0.01
3b	−1.39	2.57	0.26	1450	−0.85	0.67 ± 0.1	0.04 ± 0.01

[a] Data for CH_3CN solutions at 298 K. [b] Half-wave potentials for reduction of the coordinated diimine ligand vs SCE reference electrode. [c] Energy of relaxed MLCT excited state estimated from emission energy.[84] [d] Free energy change for electron transfer from $Co(CO)_4^-$ to MLCT excited state of Re(I) cation; see text. [e] Cage escape efficiency for 355 nm excitation. [f] Cage escape efficiency for 532 nm excitation.

absorption experiments indicate that the cage escape yield is comparatively large under MLCT excitation; however, the yield is diminished by more than an order of magnitude when direct IPCT excitation is applied. The origin of this dramatic wavelength dependence is discussed in terms of the structures of the geminate radical pairs produced by MLCT and IPCT excitation and the effect of spin-multiplicity on the rate of charge recombination.

Results

Photophysical and Electrochemical Properties of Re(I) Cations and $Co(CO)_4^-$. In order to document the properties of the Re(I) cations, the photophysics and electrochemistry of complexes **1b**, **2b**, and **3b** were examined. First, cyclic voltammetry indicates that each salt displays a reversible wave due to the first reduction of the complex, eq 1.[47] The potentials

$$(b)Re^{I}(CO)_3(py)^+ + e^- \rightarrow (b^{\bullet-})Re^{I}(CO)_3(py) \qquad (1)$$

for these reversible couples are listed as $E_{1/2}$(b/b$^{\bullet-}$) in Table 1.[56] Inasmuch as the LUMO of the complexes is the π^* molecular orbital of the diimine ligand,[58−62] the added electron is localized primarily on that ligand in the reduced complexes. It follows then that the first reduction potential of complexes **1b**, **2b**, and **3b** reflects the LUMO energy of the diimine ligand.[61,62] Note that the absolute values of $E_{1/2}$(b/b$^{\bullet-}$) follow the trend **1b** < **2b** < **3b** which indicates that the LUMO energies increase along the series. This trend reflects the fact that the electron withdrawing 4,4′-carbomethoxy substituents lower the LUMO energy while the electron donating 5,5′,4,4′-methyl substituents raise the LUMO energy compared to unsubstituted bipyridine.

As noted above, complexes **1b**, **2b**, and **3b** each display a moderately strong yellow-orange dπ (Re) → π^* (diimine) MLCT luminescence when excited with near-UV light. Estimated 0−0 energies for the relaxed MLCT state are calculated from the luminescence bands (Table 1); note that the MLCT state energy increases along the series **1b** < **2b** < **3b**, consistent with the relative ordering of the diimine LUMO energies. Emission quantum yields and lifetimes for complexes **1b**, **2b**, and **3b** are also listed in Table 1; these parameters vary in a manner consistent with the energy gap law as discussed in detail by Meyer and co-workers.[48]

Kochi and co-workers examined the absorption spectrum and electrochemistry of $Co(CO)_4^-$ in solution with the "spectator" cation $Ph_3P{=}N{=}PPh_3^+$.[52,63] Their results indicate that $Co(CO)_4^-$ does not absorb appreciably at λ > 320 nm. The $Co(CO)_4^-$ ion features an irreversible anodic wave at $E_p \approx +0.30$ V due to oxidation of the anion to the 17 e$^-$ radical, eq 2,[63] and detailed electrochemical studies suggest that the thermodyanamic potential for the oxidation is $E° = +0.33$ V vs SCE.[52,63]

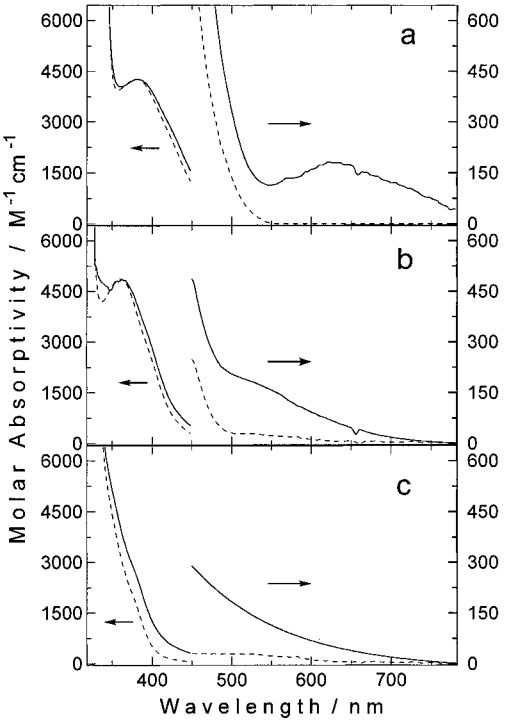

Figure 1. UV−visible absorption spectra for THF solutions: solid lines, Re(I) cations with $Co(CO)_4^-$ anion (**1a**, **2a**, and **3a**); broken lines, Re(I) cations with PF_6^- anion (**1b**, **2b**, and **3b**). (a) Complexes **1a** and **1b**, (b) complexes **2a** and **2b**, and (c) complexes **3a** and **3b**.

$$Co(CO)_4^- \rightarrow Co(CO)_4^{\bullet} + e^- \qquad (2)$$

Synthesis of Re^+, Co^- Salts. The $(b)Re^{I}(CO)_3(py)^+$ cations as salts with "inert" anions such as PF_6^- or Cl^- are pale-yellow (b = tmb)[56] to orange-yellow (b = dmeb)[56] in the solid state and in solution. However, immediately upon mixing a yellow aqueous methanolic solution of $(b)Re^{I}(CO)_3(py)^+Cl^-$ with a colorless aqueous solution of $Na^+Co(CO)_4^-$, a deep red-yellow (b = tmb) to red-orange (b = dmeb) solid precipitates. The instantaneous appearance of the strongly colored products suggests the existence of a charge transfer interaction that is unique to salts which pair $(b)Re^{I}(CO)_3(py)^+$ with the $Co(CO)_4^-$. Indeed, analysis of the salts indicates that they consist of $(b)Re^{I}(CO)_3(py)^+$ and $Co(CO)_4^-$ paired in 1:1 stoichiometry.

UV−Visible Absorption Spectra of Re^+, Co^- Salts. Ion-Pair Charge Transfer Absorption and Ion-Pair Dissociation Constants. Support for the existence of a charge transfer interaction between $(b)Re^{I}(CO)_3(py)^+$ and $Co(CO)_4^-$ comes from comparison of UV−visible absorption spectra of complexes **1a**, **2a**, and **3a** with those of the corresponding PF_6^- salts **1b**, **2b**, and **3b** (Figure 1, all spectra in THF solution). First, in the blue to near-UV region (λ < 450 nm) all of the complexes display a moderately intense absorption band ($\epsilon_{max} \approx 4000-5000$ M^{-1} cm^{-1}). This band is typically observed in

(59) Worl, L. A.; Duesing, R.; Chen, P.; Della Ciana, L.; Meyer, T. J. *J. Chem. Soc., Dalton Trans.* **1991**, 849.
(60) Schanze, K. S.; MacQueen, D. B.; Perkins, T. A.; Cabana, L. A. *Coord. Chem. Rev.* **1993**, *122*, 63.
(61) Lever, A. B. P. *Inorg. Chem.* **1991**, *30*, 1980.
(62) Dodsworth, E. A.; Vlcek, A. A.; Lever, A. B. P. *Inorg. Chem.* **1994**, *33*, 1045.
(63) Lee, K. Y.; Kochi, J. K. *Inorg. Chem.* **1989**, *28*, 567.

Table 2. Properties of Ion Pairs in THF Solution

complex	λ_{max}[a]/nm	K_d[b]/($M^{-1} \times 10^{-6}$)	ϵ_{max}[c]/M^{-1} cm^{-1}
1a	630 ± 10	6.0	320
2a	525 ± 25	3.0	230
3a	450 ± 25	2.0	120

[a] Estimated absorption maximum for IPCT absorption band. [b] Dissociation constant for contact ion pair, determined as described in experimental section. [c] Molar absorptivity for IPCT absorption band, determined as described in Experimental Section.

Table 3. Crystallographic Data for Compound **2a**

mol formula	$[ReC_{18}H_{13}N_3O_3][Co(CO)_4]$	T	25 °C
MW	676.48 g mol^{-1}	λ	0.710 73 Å
space group	$P2_1/c$ (No. 14)	Z	8
a	8.554(1) Å	ρ_{calc}	1.888 g cm^{-3}
b	28.807(4) Å	μ	58.3 cm^{-1}
c	19.498(3) Å	$R(F_o)^a$	0.057
β	97.86(1)°	$R_w(F_o)^b$	0.056
V	4759(1) $Å^3$		

[a] $R = \sum(||F_o| - |F_c||)/\sum|F_o|$. [b] $R_w = [\sum w(|F_o| - |F_c|)^2/\sum|F_o|^2]^{1/2}$.

(diimine)$Re^I(CO)_3L$ complexes and is due to the dπ (Re) → π^* (diimine) MLCT transition.[58−60] The MLCT absorption is clearly resolved in the spectra of complexes **1a**, **1b**, **2a**, and **2b**; however, it appears only as a shoulder on the more intense UV band (not shown) that is due to π,π^* intraligand absorption of the tmb ligand in complexes **3a** and **3b**. Consistent with the MLCT assignment, the band energy increases as $E_{1/2}(b/b^{\bullet-})$ becomes more negative. Furthermore, the energy and band shape of the MLCT absorption is virtually the same for corresponding PF_6^- and $Co(CO)_4^-$ salts, indicating that the MLCT transition is unaffected by the $Co(CO)_4^-$ anion.

A low-intensity, broad absorption band appears in the visible region in the spectra of $Co(CO)_4^-$ salts **1a**, **2a**, and **3a** that does not have a counterpart in the spectra of the corresponding PF_6^- salts. Several features peculiar to this absorption indicate that it arises from an IPCT transition.[50,51] First, this transition is associated with the $Co(CO)_4^-$ anion, since the band is not observed in the spectra of the corresponding PF_6^- salts **1b**, **2b**, and **3b**. However, the transition is not due to isolated $Co(CO)_4^-$, as this species does not absorb for $\lambda > 320$ nm.[52,63] The intensity and bandwidth of the mid-visible absorption band ($\epsilon_{max} \approx 100-300$ M^{-1} cm^{-1}; fwhm ≈ 5000 cm^{-1}) is similar to that of IPCT absorption bands displayed by other salts in which an electron poor (acceptor) cation is paired with an electron rich (donor) anion.[50,51] Finally, the energy of the mid-visible absorption feature increases as $E_{1/2}(b/b^{\bullet-})$ becomes more negative, consistent with a $Co(CO)_4^-$ → diimine IPCT assignment.

In solution the $Co(CO)_4^-$ salts **1a**, **2a**, and **3a** exist in an equilibrium between a contact ion pair and free ions (or solvent separated ions), eq 3. The method of Drago and Rose[52,64,65]

$$(b)Re^I(CO)_3(py)^+, Co(CO)_4^- \overset{K_d}{\rightleftharpoons} (b)Re^I(CO)_3(py)^+ + Co(CO)_4^- \quad (3)$$

was applied to determine equilibrium constants for dissociation of the contact ion pairs (K_d) and extinction coefficients for the IPCT absorption (ϵ_{max}) of complexes **1a**, **2a**, and **3a** in THF solution, and the data are collected together along with estimated λ_{max} values in Table 2. The ϵ_{max} values for **1a**, **2a**, and **3a** are comparable to those for the contact ion pair $Q^+Co(CO)_4^-$,[52] consistent with the $Co(CO)_4^-$ → diimine IPCT assignment. However, the K_d values are smaller than those for the quinolinium salt by over an order of magnitude. This latter effect may be due to poor solvation of the $(b)Re^I(CO)_3(py)^+$ cations by the low-polarity THF solvent.

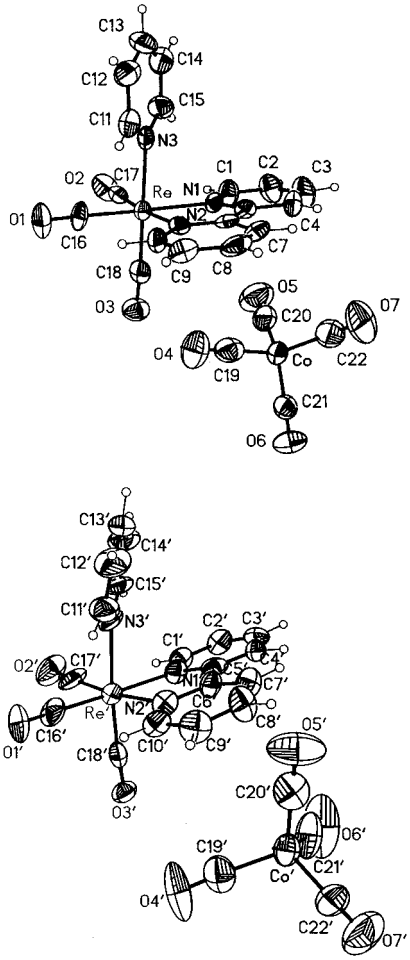

Figure 2. (a, top) ORETP diagram of ion pair $\mathbf{2a}_1$. (b) ORETP diagram of ion pair $\mathbf{2a}_2$.

X-ray Crystal Structure of Complex 2a. In order to provide further information concerning the interaction responsible for the charge transfer absorption observed in complexes **1a**, **2a**, and **3a**, an X-ray crystal structure was obtained on complex **2a**.[66] The crystal packing diagram (see Supporting Information) reveals the presence of two unique ion pairs within the unit cell. The ORTEP diagrams in Figure 2 were created by extracting each of the unique ion pairs from the surrounding atoms in the unit cell. Comparison of the data in Figure 2 and in Table 4 indicates that the structures of $(bpy)Re^I(CO)_3(py)^+$ and $Co(CO)_4^-$ are qualitatively similar in the two ion pairs; they differ mainly with respect to the relative geometry between the cation and anion partners. In ion pair $\mathbf{2a}_1$ (Figure 2a), $Co(CO)_4^-$ lies directly below the 2,2′-bipyridine ligand on the Re cation, with two of the four CO ligands pointed directly at the bipyridine nitrogens. The close proximity of $Co(CO)_4^-$ and bipyridine in complex $\mathbf{2a}_1$ is underscored by the short through space distances between N1−O5 and N2−O4 (3.32 and 3.26 Å, respectively). In ion pair $\mathbf{2a}_2$ (Figure 2b), $Co(CO)_4^-$ lies approximately in the plane defined by the bipyridine ligand and is displaced in space away from the Re cation. This qualitative comparision of the two ion-pair geometries strongly implies that the charge transfer interaction responsible for the unusual color

(64) Benesi, H. A.; Hildebrand, J. H. *J. Am. Chem. Soc.* **1948**, *70*, 2832.
(65) Rose, N. J.; Drago, R. S. *J. Am. Chem. Soc.* **1959**, *81*, 6138.

(66) The crystal packing diagram, a complete listing of bond lengths and angles, anisotropic thermal parameters, and positions of H-atoms are provided as Supporting Information. In the tabular data the two unique ion pairs in the unit cell are labeled $\mathbf{2a}_1$ and $\mathbf{2a}_2$ to allow their distinction.

Table 4. Selected Bond Lengths (Å) and Angles (deg) for Heavy Atoms

atom			**2a**$_1$[a]		**2a**$_2$[b]		**4**[c]	
1	2	3	1−2/Å	1−2−3/deg	1−2/Å	1−2−3/deg	1−2/Å	1−2−3/deg
C1	N1	C5	1.34(2)	119.7(14)	1.35(2)	117.2(14)	1.35(1)	n/a
C5	N1	Re	1.37(2)	115.0(10)	1.36(2)	115.5(10)	1.36(1)	n/a
C6	N2	C10	1.34(2)	120.7(14)	1.38(2)	119.4(14)	1.27(1)	n/a
C10	N2	Re	1.33(2)	123.0(11)			1.37(2)	n/a
C16	O1		1.11(2)		1.10(2)		1.23(2)	n/a
C17	O2		1.14(2)		1.14(2)		1.25(2)	n/a
C18	O3		1.19(3)		1.16(2)		1.16(1)	n/a
C19	Co	C20	1.75(3)	107.0(11)	1.78(2)	112.5(10)	*d*	*d*
C19	Co	C21		113.5(10)		108.4(10)	*d*	*d*
C20	Co	C21	1.75(2)	106.3(11)	1.73(2)	107.4(10)	*d*	*d*
C20	Co	C22		108.3(11)		109.5(10)	*d*	*d*
C21	Co	C22	1.74(2)	110.7(11)	1.78(2)	107.0(10)	*d*	*d*
C22	Co	C19	1.79(3)	110.6(12)	1.76(2)	111.7(10)	*d*	*d*
C19	O4		1.16(3)		1.11(3)		*d*	*d*
C20	O5		1.15(3)		1.17(3)		*d*	*d*
C21	O6		1.15(3)		1.12(3)		*d*	*d*
C22	O7		1.08(4)		1.12(3)		*d*	*d*

[a] **2a**$_1$ refers to the ion pair shown in Figure 2a. [b] **2a**$_2$ refers to the ion pair shown in Figure 2b. [c] Data for compound **4** from ref 66. [d] No comparison possible.

of the crystal of complex **2a** is embodied in the ion pair shown in Figure 2a (i.e., structure **2a**$_1$).

Table 4 contains a listing of selected bond lengths and angles for ion pairs **2a**$_1$ and **2a**$_2$, along with the corresponding parameters for the related complex [(2,2′-bipyridine)Re^{I}(CO)$_3$-(*N*-methyl-4,4′-bipyridinium)$^{2+}$][PF$_6^-$]$_2$ (compound **4**).[67] The data in Table 4 reveal that the identity and/or position of the anion has a marginal effect upon the structure of the (bpy)Re^{I}-(CO)$_3^+$ cation.[68] For example, the four C−N bond lengths in the 2,2′-bipyridine ligand are very similar in complexs **2a**$_1$, **2a**$_2$, and **4**. The lengths of the C−O bond in the carbonyl ligands at the Re cation are very similar in structures **2a**$_1$ and **2a**$_2$; however, the corresponding C−O bonds are elongated slightly in the carbonyls that are trans to 2,2′-bipyridine in **4**. This may be a secondary effect due to the presence of the *N*-methyl-4,4′-bipyridinium ligand (a stronger π-back-bonding ligand than pyridine) in complex **4**. In both complexes **2a**$_1$ and **2a**$_2$ Co(CO)$_4^-$ exists in a slightly distorted tetrahedral geometry. However, the bond lengths and angles for the two unique Co(CO)$_4^-$ species in structures **2a**$_1$ and **2a**$_2$ are not distorted in a systematic manner, which could be attributed to the existence of a charge transfer interaction.

Luminescence Properties of Re$^+$, Co$^-$ Salts. As noted above, the (b)Re^{I}(CO)$_3$(py)$^+$ cations exhibit yellow-orange luminescence which is attributed to the MLCT excited state.[58−60] Thus, the luminescence properties of complexes **2a** and **3a** were examined in detail in order to investigate the effect of the moderately strong electron donor Co(CO)$_4^-$ anion on the MLCT state. Very similar effects were observed for complexes **2a** and **3a**; therefore, in the interest of brevity we present only detailed data for complex **2a**.

The MLCT luminescence of complexes **2a** and **2b** ($c = 2.0 \times 10^{-5}$ M) in THF and CH$_3$CN solution was compared. Although the MLCT emission maximum of both salts is slightly red-shifted in CH$_3$CN relative to THF ($\lambda_{max}^{CH_3CN} = 589$ nm, $\lambda_{max}^{THF} = 587$ nm), the emission band shape and energy are exactly the same for **2a** and **2b** in the same solvent. This correspondence indicates that Co(CO)$_4^-$ does not significantly perturb the MLCT state. However, in both solvents the emission intensity for complex **2a** is lower relative to that of complex **2b**, which implies that Co(CO)$_4^-$ quenches the MLCT excited state. It is likely that luminescence quenching is due to photoinduced electron transfer, from Co(CO)$_4^-$ to the MLCT excited state Re cation, eq 4. In accord with this hypothesis,

$$(b^{\bullet-})Re^{II}(CO)_3(py)^{+}* + Co(CO)_4^- \rightarrow (b^{\bullet-})Re^{I}(CO)_3(py) + Co(CO)_4^{\bullet} \quad (4)$$

the electrochemical and luminescence data on (bpy)Re^{I}(CO)$_3$-(py)$^+$ and Co(CO)$_4^-$ indicate that photoinduced electron transfer is strongly exothermic (ΔG_{fet} in Table 1, *vide infra*).[69] Another important feature is that the emission intensity of complex **2a** is more strongly quenched in THF than in CH$_3$CN. This implies that static quenching may be important for complex **2a** in THF, consistent with the fact that complex **2a** exists predominantly as ion pairs in this relatively nonpolar solvent.

Table 5. Concentration Dependence of Emission Properties of Complex **2a** in THF[a]

[**2a**]/μM	I_{em}(**2a**)/I_{em}(**2b**)[b]	τ_{em}(**2a**)/τ_{em}(**2b**)[c]	[**2a**]/μM	I_{em}(**2a**)/I_{em}(**2b**)[b]	τ_{em}(**2a**)/τ_{em}(**2b**)[c]
6.6	0.87	0.69	330	0.03	0.13
33	0.29	0.47	660	<0.005	0.085
66	0.17	0.35			

[a] Argon degassed solution at 298 K. [b] Ratio of emission intensity for solutions of complexes **2a** and **2b** having matched optical density at the excitation wavelength. [c] Ratio of emission lifetime of complex **2a** to complex **2b** (τ(**2b**) = 234 ns).

Stern−Volmer studies were carried out on complex **2a** in order to investigate the quenching process(es) in more detail. Steady state experiments were carried out by measuring the luminescence intensity of solutions of complexes **2a** and **2b** having matched optical density at the excitation wavelength. The concentration of the two complexes was varied (in parallel) from 6.6 to 660 μM, and the results are listed in Table 5 as I_{em}(**2a**)/I_{em}(**2b**), where I_{em}(**2a**) and I_{em}(**2b**) are MLCT emission intensities of the two complexes at corresponding concentrations. Note that the luminescence intensity of complex **2a** clearly decreases with increasing concentration. A parallel study was carried out in which the emission lifetime (τ_{em}) of complex **2a**

(67) Chen, P.; Curry, M.; Meyer, T. J. *Inorg. Chem.* **1989**, *28*, 2271.
(68) This may not be surprising in view of the fact that variation of the anion typically does not have an impact on the structure of the cation in crystal structures of organic salts. For example, see ref 52, p 4671, and references cited therein.
(69) The driving force for the photoinduced electron transfer reaction in eq 4 is given by the expression $\Delta G_{fet} = E_{1/2}(b/b^{\bullet-}) - E_{1/2}(Co(CO)_4^-/Co(CO)_4^{\bullet}) - E_{MLCT}$, where the $E_{1/2}$ values represent half-wave potentials for the two couples and E_{MLCT} is the energy of the luminescent ^{3}MLCT state of the (b)Re^{I}(CO)$_3$(py)$^+$ complex.

was examined as a function of concentration.[70] Table 5 contains a listing of the lifetimes of complex **2a** relative to that of complex **2b** ($\tau_{em}^{2b} = 234$ ns, concentration independent). Note that τ_{em} for complex **2a** also decreases with increasing concentration; however, the decrease in τ_{em} is not as pronounced as that for I_{em}, consistent with static quenching.

The concentration dependent steady state and time resolved emission data listed in Table 5 were analyzed according to the Stern−Volmer equation (eqs 5a,b). In these equations k^{SS} and

$$\frac{\tau_{em}(\mathbf{2b})}{\tau_{em}(\mathbf{2a})} = 1 + k^{LT}\tau_{em}(\mathbf{2b})[\mathbf{2a}] \quad (5a)$$

$$I_{em}(\mathbf{2b})/I_{em}(\mathbf{2a}) = 1 + k^{SS}\tau_{em}(\mathbf{2b})[\mathbf{2a}] \quad (5b)$$

k^{LT} are empirical second-order rate constants for quenching derived from steady state and emission lifetime data, respectively, and $\tau_{em}(\mathbf{2b}) = 234$ ns. Plots of the experimental data according to eqs 5a,b are approximately linear, and least-squares fits yield values of $k^{LT} = 6.9 \times 10^{10}$ M^{-1} s^{-1} and $k^{SS} = 3.6 \times 10^{11}$ M^{-1} s^{-1}.

Several points are clear from the Stern−Volmer analysis. First, the fact that $k^{SS} > k^{LT}$ indicates that static quenching is important for complex **2a**. Indeed, the empirical rate constant obtained from the steady state data is even larger than the diffusion controlled limit ($k_{diff} = 1.0 \times 10^{11}$ M^{-1} s^{-1}).[71,72] Second, the quenching rate constant obtained by analysis of the lifetime data reveals that $Co(CO)_4^-$ quenches the MLCT excited state via a diffusional pathway at approximately the diffusion controlled limit, consistent with the fact that photoinduced electron transfer (eq 4) is very exothermic (Table 1). Third, the steady state Stern−Volmer analysis clearly indicates that the MLCT excited state of the $(bpy)Re^{I}(CO)_3(py)^+$ chromophore is quenched with ≥90% efficiency by $Co(CO)_4^-$ when [**2a**] ≥ 770 μM in THF solution. This point is significant, since the quantitative laser flash photolysis studies described below were carried out under these conditions.

Nanosecond Laser Flash Photolysis. Laser flash photolysis experiments were carried out on complexes **2a** and **3a** in order to compare the yields of the electron transfer products formed by MLCT and IPCT excitation. Similar results were obtained on both complexes; therefore, detailed results are presented only for complex **2a**. Figure 3 illustrates a series of transient absorption difference spectra obtained with complex **2a** or **2b**. First, Figure 3a illustrates the difference absorption spectrum of complex **2b** in THF ($c = 0.2$ mM) with 0.1 M triethylamine at 40 μs delay after 355 nm excitation. The difference spectrum of the complex **2b**/triethylamine system is characterized by two resolved bands in the UV ($\lambda_{max} = 350$ and 370 nm) and a broad absorption in the mid-visible ($\lambda_{max} = 490$ nm). Previous studies have shown that triethylamine reduces the MLCT excited state according to eq 6.[73] Inasmuch as the triethylamine radical cation

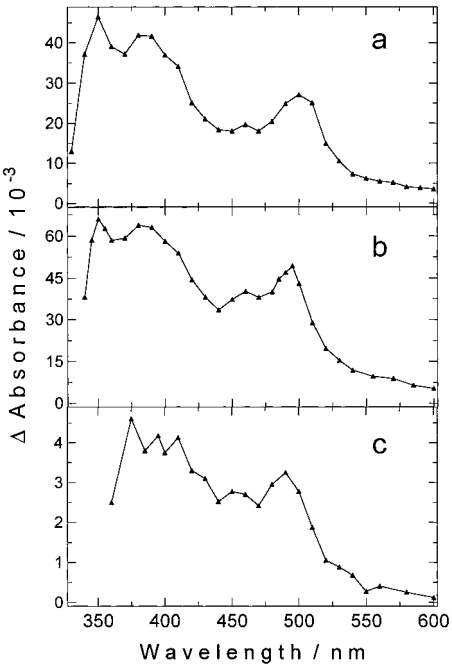

Figure 3. Transient absorption difference spectra obtained following 10 ns pulsed laser excitation, THF solutions: (a) complex **2b** with 0.1 M triethylamine, 40 μs delay following 355 nm laser pulse; (b) complex **2a**, 10 μs delay following 355 nm laser pulse; (c) complex **2a**, 10 μs delay following 532 nm laser pulse.

$$(bpy^{\bullet-})Re^{II}(CO)_3(py)^{+}* + NEt_3 \rightarrow (bpy^{\bullet-})Re^{I}(CO)_3(py) + NEt_3^{\bullet+} \quad (6)$$

(or the α-amino radical derived therefrom by deprotonation) does not absorb appreciably in the near-UV or visible region,[74] the absorption difference spectrum in Figure 3a is due exclusively to the 19 e^- complex $(bpy^{\bullet-})Re^{I}(CO)_3(py)$.[47]

Figure 3b illustrates the transient absorption difference spectrum of complex **2a** in THF ($c = 0.1$ mM) at 40 μs delay following 355 nm excitation. The near-UV excitation wavelength corresponds to the MLCT absorption band of the $(bpy)Re^{I}(CO)_3(py)^+$ chromophore. The transient absorption difference spectrum produced by 355 nm excitation of complex **2a** is virtually superimposable with that obtained by flash excitation of the complex **2b**/triethylamine system, indicating that $(bpy^{\bullet-})Re^{I}(CO)_3(py)$ is formed via photoinduced electron transfer from $Co(CO)_4^-$ (eq 4).[75] Although previous studies indicate that $Co(CO)_4^{\bullet}$ absorbs moderately at $\lambda > 760$ nm,[52] we were unable to monitor this absorption feature due to the poor sensitivity of the laser flash photolysis system for $\lambda > 720$ nm.

Figure 3c illustrates the transient absorption difference spectrum obtained by 532 nm excitation of complex **2a** in THF

(70) Careful analysis of the time resolved emission data for complex **2a** did not reveal the presence of any short-lived decay components that could be ascribed to the ion-pair. For each concentration of complex **2a**, the emission kinetics were adequately represented by a single exponential decay function.

(71) The rate of diffusional encounter was calculated by using the Debye−Stokes equation,[72]

$$k_q^{diff} = \frac{2N_A k_B T}{3\eta}\frac{(r_A + r_D)^2}{r_A r_D}\frac{b}{(e^b - 1)}$$

where $b = (Z_D Z_A e^2)/(4\pi\epsilon_0\epsilon r_{DA} k_B T)$, N_A is Avogadro's number, η is the solvent viscosity, e is the electron charge, ϵ_0 is the permittivity of free space, ϵ is the static dielectric constant of the solvent, r_{DA} is the reaction encounter distance, Z_D and Z_A are the charges on the donor (D) and acceptor (A) ions, respectively, and r_D and r_A are the radii of D and A, respectively. By using $Z_A = +1$ and $r_A = 4.2$ Å for the $(bpy)Re(CO)_3(py)^+$ acceptor, $Z_D = -1$ and $r_D = 4.7$ Å for the $Co(CO)_4^-$ donor, and $r_{DA} = r_D + r_A$, the Debye−Stokes equation predicts that in THF solution $k_q^{diff} = 1.0 \times 10^{11}$ M^{-1} s^{-1}.

(72) Laidler, K. J. *Chemical Kinetics*, 3rd ed.; Harper and Row: New York, 1987.

(73) McCosar, B. H.; Schanze, K. S. *Inorg. Chem.* **1996**, *35*, 6800.

(74) Shida, T. *Electronic Absorption Spectra of Radical Ions*; Elsevier: Amsterdam, 1988.

(75) The transient absorption of $(bpy^{\bullet-})Re^{I}(CO)_3(py)$ decays via equal-concentration, second-order kinetics with a rate of 1.0×10^9 M^{-1} s^{-1}, as expected if the metal complex decays by diffusional charge recombination with $Co(CO)_4$.

($c = 1$ mM). The 532 nm excitation directly excites the IPCT absorption of the salt. Apart from poor *S*/*N* in the near-UV region due to strong ground state absorption, the difference spectrum is very similar to those in Figure 3a,b, demonstrating that direct excitation of the $Co(CO)_4^-$ → bpy IPCT absorption also affords $(bpy^{\bullet-})Re^I(CO)_3(py)$.[75]

Quantitative transient absorption experiments were carried out on THF solutions of complexes **2a** and **3a** to determine the efficiency for formation of free radicals by excitation into the MLCT and IPCT absorptions. The cage escape yield (Φ_{esc}) of $(b^{\bullet-})Re^I(CO)_3(py)$ was determined for both systems; this species is presumably formed in 1:1 stoichiometry with the 17 e^- radical $Co(CO)_4^{\bullet}$, eq 7.

$$\mathbf{2a} \text{ or } \mathbf{3a} \xrightarrow{h\nu(\text{MLCT}) \text{ or } h\nu(\text{IPCT})} (b^{\bullet-})Re^I(CO)_3(py) + Co(CO)_4^{\bullet} \quad (7)$$

The cage escape yields were determined as described in the Experimental Section, and the results for complexes **2a** and **3a** are listed in Table 1. Interestingly, with MLCT excitation Φ_{esc} is large, but with IPCT excitation Φ_{esc} is lower by more than an order of magnitude. The origin of the strong wavelength dependence of Φ_{esc} is discussed below.

Discussion

Structure and Optical Spectra of Re^+, Co^- Salts. The unique color associated with complexes **1a**, **2a**, and **3a** in the solid state or dissolved in nonpolar solvents signals the existence of a charge transfer interaction between $Co(CO)_4^-$ and $(b)Re^I(CO)_3(py)^+$. The orbital basis for the IPCT transition derives primarily from the HOMO of $Co(CO)_4^-$ and the LUMO of $(b)Re^I(CO)_3(py)^+$. The HOMO of $Co(CO)_4^-$ consists of the triply degenerate d_{xy}, d_{xz}, and d_{yz} orbitals which are partially delocalized onto the carbonyl ligands via mixing with the π^* CO orbitals.[76] The LUMO of $(b)Re^I(CO)_3(py)^+$ is almost purely π^* diimine, with only a small contribution from $d\pi$ orbitals at Re. Thus, in a one electron approximation the IPCT transition is dominated by the configuration d (Co) → π^* (diimine). A consequence of this configuration is that IPCT excitation leads to direct "injection" of an electron from $Co(CO)_4^-$ into the π^* orbital of the diimine acceptor, e.g.,

$$(b)Re^I(CO)_3(py)^+, Co(CO)_4^- \rightarrow (b^{\bullet-})Re^I(CO)_3(py), Co(CO)_4^{\bullet} \quad (8)$$

In view of the d (Co) → π^* (diimine) assignment for the IPCT transition in complexes **1a**, **2a**, and **3a**, it is easy draw an analogy between the charge transfer interaction in these salts and those which pair $Co(CO)_4^-$ with (organic) heterocyclic cations.[52−55] The latter salts feature IPCT absorption bands which are due to optical electron transfer from carbonylcobaltate to the π^* (LUMO) of the heterocycle. An interesting feature is the close similarity in the proximity and orientation of the $Co(CO)_4^-$ anion with respect to the heterocycles in the X-ray structures of the organic ion pairs[52] and complex **2a**. Specifically, in both cases, $Co(CO)_4^-$ is positioned close to and above the plane defined by the heterocycle. For example, in ion pair $\mathbf{2a_1}$ $Co(CO)_4^-$ is located directly above bpy, with the carbonyl oxygens positioned so that they are nearly in contact with the bpy nitrogens. By analogy, in the X-ray structure of $Q^+Co(CO)_4^-$, the tetracarbonylcobaltate anion lies directly above the plane defined by the quinolinium cation, and there is a relatively small distance separating the Co atom and the heterocyclic ring.[52]

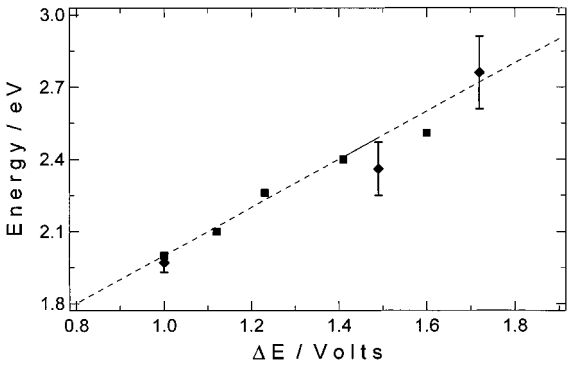

Figure 4. Plot of energy of CT absorption band maximum vs ΔE for THF solutions. Polygons with error bars represent data for complexes **1a**, **2a**, and **3a**. Squares represent data for $Q^+Co(CO)_4^-$ salts (from ref 52).

An interesting question concerns the pathway for electronic interaction between $Co(CO)_4^-$ and $(b)Re^I(CO)_3(py)^+$ in complexes **1a**, **2a**, and **3a**. While ion pair $\mathbf{2a_1}$ which is present in the crystalline state likely embodies the structural features necessary for the charge transfer interaction (e.g., the crystal is red due to IPCT absorption), careful analysis of the structural parameters for this ion pair does not reveal obvious geometric distortions that can be ascribed to the charge transfer interaction.[68] In spite of this fact, on the basis of the X-ray structure we postulate that the HOMO−LUMO overlap that is necessary for the IPCT transition is likely mediated primarily via interaction of the carbonyl oxygens and the p orbitals located at the bpy nitrogens. The carbonyl groups may act as a "bridge" for charge transfer from Co → bpy because the HOMO of the carbonylmetallate is partially delocalized into the p orbitals on the oxygen atoms.

The structural and electronic similarity of the ion pairs reported by Bockman and Kochi and complexes **1a**, **2a**, and **3a** is underscored by the correlation of E_{IPCT} vs $\Delta E_{1/2}$ shown in Figure 4, where E_{IPCT} is the estimated energy of the IPCT band maximum and $\Delta E_{1/2}$ is the difference between the $E_{1/2}$ values for for reduction of the acceptor cations and oxidation of $Co(CO)_4^{\bullet-}$ Note that there is good qualitative agreement between the correlations defined by the two series of compounds. This strongly supports the hypothesis that the visible absorption band in complexes **1a**, **2a**, and **3a** arises from d (Co) → π^* (diimine) charge transfer.

The energy of an ion pair charge transfer absorption band is given by eq 9, where ΔG_w is the free energy for dissociation of the ion pair into free ions, χ is the reorganization energy for the optical transition, and the other parameters are defined above.[50,51] This equation predicts that a plot of E_{IPCT} vs $\Delta E_{1/2}$

$$E_{IPCT} = \Delta E_{1/2} - \Delta G_w + \chi \quad (9)$$

will be linear with unit slope and an intercept of $\chi - \Delta G_w$. Consistent with the prediction of eq 9, the solid line drawn through the experimental data in Figure 4 has a slope of 1.0 and *y*-intercept of 1.0 eV. Taking a value of $K_d = 10^{-5}$ M^{-1} for the ion-pair dissociation constant leads to a value of $\Delta G_w = 0.30$ eV; this value coupled with the intercept of the correlation shown in Figure 4 implies that $\chi = 0.7 \pm 0.1$ eV for the IPCT absorption in the carbonylcobaltate ion pairs. Interestingly, this experimentally determined χ value is in good agreement with that calculated by using the Marcus−Hush two sphere model ($\chi_{theory} = 0.6$ eV).[77,78]

(76) Extended Huckel calculations were carried out using HyperChem (version 4.0, HyperCube, Inc.) running on a Micron Intel P160 microcomputer under Windows 95.

Scheme 1

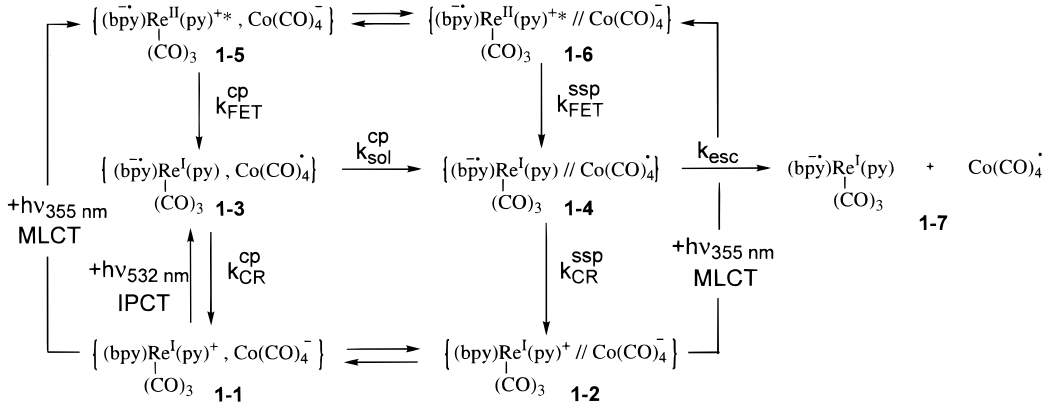

Mechanism of Photoinduced Charge Transfer in Ion Pairs. Transient absorption studies clearly indicate that near-UV or visible excitation of complex **2a** or **3a** produces $(b^{\bullet-})Re^{I}(CO)_3(py)$. However, the quantitative transient absorption studies show that the yield of this reactive intermediate is large with MLCT excitation and small with IPCT excitation. An important question that must be addressed concerns the origin of this effect. Two plausible mechanisms that explain the wavelength dependent yields are described below; both find precedent in earlier work on photoinduced electron transfer reactions in metal complexes and organic donor−acceptor systems.

The first mechanism (Scheme 1) is distinguished by recognizing that in the ground or excited state there is an equilibrium distribution of contact and solvent separated ion pairs. Specifically, ground and excited state ions exist either as contact pairs (**1**−**1** and **1**−**5**) or solvent separated pairs (**1**−**2** and **1**−**6**). By analogy, geminate pairs formed by photoinduced electron transfer exist either as contact or solvent separated radical pairs (**1**−**3** and **1**−**4**, respectively). Only free radicals that successfully undergo cage escape (e.g., **1**−**7**) are detected by nanosecond laser flash. An important distinction between the two types of ground state ion pairs is that since electronic coupling between the donor and acceptor is lower in the solvent separated pair **1**−**2**, only contact pair **1**−**1** exhibits an IPCT absorption band. Thus, IPCT excitation selectively excites only contact pairs, giving rise directly to the contact radical pair state (e.g., **1**−**1** + $h\nu_{532}$ → **1**−**3**). By contrast, MLCT excitation is nonselective and produces both photoexcited contact and solvent separated pairs (e.g., **1**−**1** + $h\nu_{355}$ → **1**−**5** *and* **1**−**2** + $h\nu_{355}$ → **1**−**6**). The most important consequence of the nonselective nature of MLCT excitation is that "long-range electron transfer" (LRET) can occur within the solvent separated pair **1**−**6**, giving rise directly to the solvent separated geminate pair **1**−**4**.[6,9,10]

The model presented in Scheme 1 provides a means for rationalizing the difference in free radical yields for IPCT versus MLCT excitation. First, it is important to point out that the donor−acceptor electronic coupling is larger within the contact geminate pair (**1**−**3**) compared to the solvent separated geminate pair (**1**−**4**). Consequently, with the assumption that the reorganization energy is not significantly different for the two types of geminate pairs, charge recombination will be faster in the contact pairs (e.g., $k^{cp}_{CR} > k^{ssp}_{CR}$). This factor alone could account for the increased free radical yield for MLCT vs IPCT excitation. This is because IPCT excitation selectively produces contact pairs which may recombine at an accelerated rate, while MLCT excitation may lead to population of solvent separated pairs which have a greater propensity to cage escape because of their intrinsically slower charge recombination rate. However, in addition to this effect, another factor will also act to augment the cage escape yield for MLCT excitation. This secondary effect arises because cage escape from the contact radical pair requires two steps: solvation (e.g., **1**−**3** → **1**−**4**), followed by cage escape (e.g., **1**−**4** → **1**−**7**). Importantly, since charge recombination may occur for both contact and solvent separated radical pairs, those pairs that are born as contact pairs can recombine at either of two stages on the way to cage escape. By contrast, solvent separated pairs (**1**−**4**) produced directly via MLCT excitation followed by LRET can cage escape directly.

The second mechanism that may explain the difference in cage escape yields is illustrated in Scheme 2. This scheme focuses explicitly upon the effect of electronic spin state on charge recombination and cage escape rather than the structure of the ion pairs (e.g., contact vs solvent separated). Although spin−orbit coupling is clearly very large in the $(b)Re^{I}(CO)_3(py)^{+}$ chromophore, it is generally accepted that the lowest, luminescent MLCT excited state is predominantly a triplet.[79] Thus, excitation into the near-UV MLCT absorption band produces a singlet MLCT state which rapidly ($k \geq 10^{12}$ s^{-1}) intersystem crosses to the lowest triplet MLCT state. This process is illustrated for ion pair **2a** in Scheme 2, where MLCT excitation of ground state ion pair **2**−**1** promptly affords ion pair **2**−**2** in which the $(b)Re^{I}(CO)_3(py)^{+}$ chromophore is in the triplet MLCT excited state. When electron transfer occurs within ion pair **2**−**2**, the product is geminate radical pair **2**−**3**, which retains the triplet spin character of the MLCT excited state. Now, since geminate pair **2**−**3** is born as a triplet, charge recombination can only occur after the geminate pair undergoes a triplet → singlet (T → S) spin transition to singlet pair **2**−**4** ($k_{T\rightarrow S}$ step, Scheme 2).[57] However, since the T → S transition may be comparatively slow, cage escape from triplet geminate pair **2**−**3** is very competitive and the net result is that free radicals (**2**−**5**) are produced efficiently via MLCT excitation. The situation is markedly different when ground state ion pair

(77) The outer sphere reorganization energy (χ) was calculated by using the Marcus−Hush two sphere model,[78]

$$\chi = \frac{\Delta q^2}{4\pi\epsilon_0}\left[\frac{1}{2r_D} + \frac{1}{2r_A} - \frac{1}{r_{DA}}\right]\left[\frac{1}{\epsilon_{op}} - \frac{1}{\epsilon_s}\right]$$

where q is the charge transferred, ϵ_0 is the permittivity of free space, r_D and r_A are the radii of the donor and acceptor, respectively, r_{DA} is the center to center D−A separation distance, and ϵ_{op} and ϵ_s are the optical and static dielectric constants of the medium, respectively. In the calculation, r_D = 4 Å, r_A = 5 Å, r_{DA} = 9 Å, and the other parameters are appropriate for THF solvent.

(78) Marcus, R. A.; Sutin, N. *Biochim. Biophys. Acta* **1985**, *811*, 265.

(79) Striplin, D. R.; Crosby, G. A. *Chem. Phys. Lett.* **1994**, *221*, 426.

Scheme 2

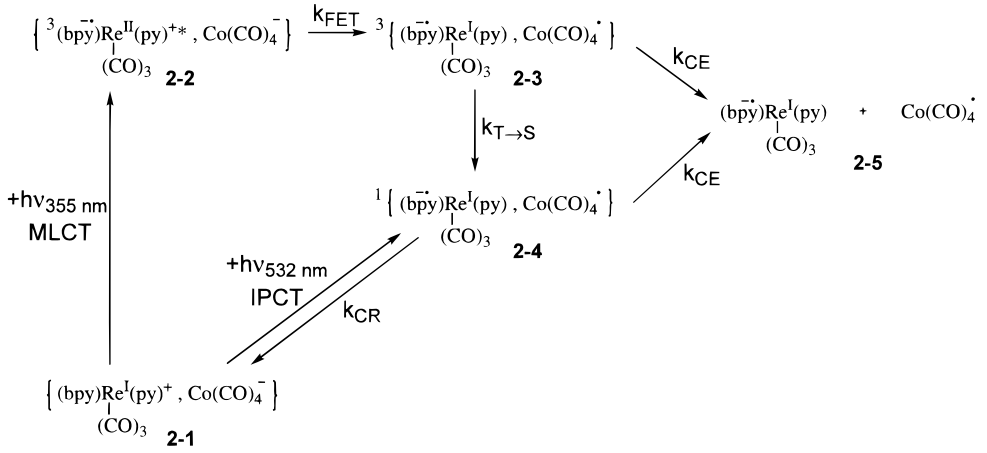

2−**1** is excited directly into the IPCT band. In this case the singlet state geminate pair **2**−**4** is produced directly. Consequently, charge recombination is spin allowed and occurs rapidly, leading to a low cage escape yield.

While each of the two mechanisms in Schemes 1 and 2 provides an explanation for the strong wavelength dependence of Φ_{esc} in complexes **2a** and **2b**, we believe that the electronic spin state of the geminate radical pairs (Scheme 2) is the overriding factor. There is only a limited amount of direct experimental evidence concerning the electronic spin state of geminate radical (ion) pairs produced by photoinduced electron transfer from MLCT excited states of Ru(II), Os(II), and Re(I) complexes.[45−47,57] However, the available evidence implies that, in these systems, (1) geminate radical (ion) pairs are born as triplets and (2) the rate of back electron transfer within geminate pairs is restricted by the requirement that a T → S spin transition precedes electron transfer. The most significant line of experimental evidence comes from studies of the magnetic field dependence of Φ_{esc} in the $Ru(bpy)_3^{2+}$/dimethylviologen system.[57] In this system it has been demonstrated that Φ_{esc} decreases with increasing magnetic field strength (for field strengths ranging from 0 to 3.5 T). The decrease in Φ_{esc} has been attributed to a magnetic field-induced increase in the rate of the T → S transition in the geminate radical ion pair produced by photoinduced electron transfer from $Ru(bpy)_3^{2+}$* to dimethylviologen.[57] The increased rate of the spin transition results in an increase in the "effective" rate of back-electron transfer and a concomitant decrease in Φ_{esc}.

Given that magnetic field effects on Φ_{esc} have been observed in d^6 metal complex systems when triplet geminate pair states are involved, a preliminary study was carried out to determine whether such effects could be detected in complex **2a** (355 nm excitation). However, a magnetic field effect was not observed on Φ_{esc} for field strengths ranging from 0 to 0.05 T. This result is not surprising given the relatively low magnetic field strengths used in the experiment. Typically magnetic field effects on Φ_{esc} are observed for field strengths of less than 0.1 T only when the T → S conversion is dominated by electron−nuclear (hyperfine) coupling.[80,81] On the other hand, when the T → S conversion is dominated by spin−orbit coupling, large magnetic field strengths (e.g., >0.5 T) are required to elicit an effect on Φ_{esc}.[57] Thus, failure of the preliminary magnetic field experiment on complex **2a** does not rule out the involvement of triplet geminate pairs in the photoinduced electron transfer reaction; rather it implies that spin−orbit coupling may be the dominant term in the T → S conversion.

If one assumes that the mechanism in Scheme 2 accurately describes the properties of geminate radical pairs produced by MLCT and IPCT excitation of complex **2a** (and complex **3a**), then it is possible to use the experimental Φ_{esc} values to estimate effective charge recombination rates within these geminate pairs. Inasmuch as triplet geminate pair **2**−**3** (which is produced by MLCT excitation) must undergo a T → S spin transition before charge recombination, the effective rate of charge recombination amounts to a "composite" of the rates of the spin transition and charge recombination.[82] The effective rate of charge recombination (k_{CR}) is related to Φ_{esc} by eq 10, where k_{CE} is the rate

$$k_{CR} = k_{CE}\left(\frac{1}{\Phi_{esc}} - 1\right) \qquad (10)$$

by which the $(b^{\bullet-})Re^{I}(CO)_3(py)$ and $Co(CO)_4^{\bullet}$ radicals escape the geminate pair. The Eigen equation (eq 11) can be used to

$$k_{CE} = \frac{k_B T}{2\pi\eta(r_A + r_D)^2}\left(\frac{1}{r_A} + \frac{1}{r_D}\right) \qquad (11)$$

estimate k_{CE},[72] where terms involving Coulombic interaction are set equal to 1 because the Re and Co radicals are uncharged, k_B is the Boltzmann constant, T is absolute temperature, η is the solvent viscosity, and r_A and r_D are the radii of the $(b^{\bullet-})Re^{I}(CO)_3(py)$ and $Co(CO)_4^{\bullet}$ radicals (ca. 4 Å). Inserting values that are appropriate for complex **2a** (THF solvent, T = 298 K) into the Eigen equation leads to an estimate of $k_{CE} = 1 \times 10^{10}$ s^{-1}. Finally, inserting the experimental values of Φ_{esc} for complex **2a** and $k_{CE} = 1 \times 10^{10}$ s^{-1} into eq 10 leads to estimates of $k_{CR}^{MLCT} = 4 \times 10^{9}$ s^{-1} for the triplet geminate pair (**2**−**3**, Scheme 2) and $k_{CR}^{IPCT} = 2 \times 10^{11}$ s^{-1} for the singlet contact geminate pair (**2**−**4**, Scheme 2).

It is useful to compare the rates for charge recombination following MLCT and IPCT excitation of complex **2a** with charge recombination rates for analogous systems. First, we recently carried out a detailed study of Φ_{esc} for bimolecular photoinduced electron transfer from diaza[2.2.2]bicyclooctane (DABCO) to the MLCT excited state of a series of $(b)Re^{I}(CO)_3(py)^+$ complexes:[47]

$$(b^{\bullet-})Re^{II}(CO)_3(py)^{+}* + DABCO \rightarrow (b^{\bullet-})Re(CO)_3(py) + DABCO^{\bullet+} \qquad (12)$$

(80) Nolting, F.; Staerk, H.; Weller, A. *Chem. Phys. Lett.* **1982**, *88*, 523.
(81) Weller, A.; Nolting, F.; Staerk, H. *Chem. Phys. Lett.* **1983**, *96*, 24.

(82) It is likely that charge recombination is faster than the rate of the T → S transition in the geminate radical pair. Thus, the effective rate of charge recombination is probably determined by the rate of the spin transition.

The cage escape yields in this system are comparable to those observed for MLCT excitation of ion pairs **2a** (and ion pair **3a**). Since the cage escape rates for the geminate pairs [(b$^{\bullet-}$)Re(CO)$_3$(py), DABCO$^{\bullet+}$] and [(b$^{\bullet-}$)Re(CO)$_3$(py), Co(CO)$_4^{\bullet}$] are likely similar, the correspondence in Φ_{esc} for the two systems implies that the rate of charge recombination is also comparable. Thus, the effective charge recombination rate for MLCT excitation of complex **2a** (k_{CR}^{MLCT}) is qualitatively similar (e.g., within a factor of 2−3) to that observed when the MLCT excited state is quenched by DABCO via diffusion controlled bimolecular electron transfer. This correspondence suggests that the T → S conversion is the dominant factor in governing the rate of charge recombination (and therefore the cage escape efficiency) in both systems.

Next, we compare k_{CR}^{IPCT} for complex **2a** with charge recombination rates for contact ion−radical pairs produced by excitation of ground state organic donor−acceptor charge transfer complexes. A number of studies have been carried out on these systems, and it has generally been found that[3−28] (1) charge recombination rates in contact radical ion pairs produced by charge transfer excitation generally range from 10^{10} to 10^{11} s^{-1} and (2) charge recombination rates generally increase with decreasing driving force, in accord with expectation for highly exothermic (Marcus inverted region) electron transfer. The estimated rate for charge recombination in singlet contact radical pairs produced by IPCT excitation of complex **2a** (k_{CR}^{IPCT}) is in reasonable agreement with the rates observed in the organic donor−acceptor systems, which again points to a similarity in the mechanism, e.g., that in each case spin-singlet, contact geminate radical (ion) pairs are produced and are able to directly undergo charge recombination.

Experimental Section

Reagents and Previously Reported Compounds. Reagent grade solvents and chemicals were used for synthesis without purification unless otherwise noted. Chromatography was carried out on either silica gel (Merck, 230−400 mesh) or Brockman grade III neutral alumina (Fisher Chemical Co.). NMR spectra were run on Bruker QE-300 or Varian Gemini 300 NMR spectrometers. Metal complex **2b** was prepared via reaction of (bpy)Re(CO)$_3$(CF$_3$SO$_3$) with pyridine as described previously.[83,84] Metal complexes **1b** and **3b** were prepared from the corresponding chloro- complexes (dmeb)Re(CO)$_3$Cl and (tmb)-Re(CO)$_3$Cl by reaction with pyridine in the presence of $AgPF_6$ as decribed previously.[85] $NaCo(CO)_4$ was prepared according to the method of Edgell and Lyford.[86]

General Procedure for Preparation of Rhenium(I) Tetracarbonylcobaltate Salts. (a) PF_6^- to Cl^- Metathesis of Complexes 1b, 2b, and 3b. Dowex anion exchange resin (7.0 g, Dowex 1X2-100, Aldrich Chemical Co.) was suspended in CH_3OH and allowed to soak for at least 1 h. The presoaked resin was then packed into a chromatography column (ca. 10 cm height × 1.5 cm diameter) and washed, first with 50 mL of a CH_3OH solution containing tetramethylammonium chloride (c = 50 mM) and second with 100 mL of neat CH_3OH. Then 100 mg of complex **1b**, **2b**, or **3b** was dissolved in 25 mL of CH_3OH/CH_3CN (4:1 (v:v)), and the metal complex solution was eluted through the resin-packed column using excess CH_3OH/CH_3CN (4:1 (v:v)) as eluant. The yellow solution collected from the column was concentrated under reduced pressure leaving the Cl^- form of the complex as an oily, yellow solid. This material was used directly in the following procedure.

(b) Preparation of Rhenium(I) Tetracarbonylcobaltate Salts 1a, 2a, and 3a. The following procedure is written specifically for preparation of complex **2a**; however, the same procedure was followed for preparation of complexes **1a** and **3a**. Freshly prepared $NaCo(CO)_4$ (35 mg, 0.18 mmol, 1.3 equiv) was weighed into a Schlenk tube in an argon purged drybox. The Schlenk tube was removed from the drybox and installed onto a Schlenk line, whereupon 4 mL of degassed H_2O was transferred by cannula to a Schlenk tube containng the $NaCo(CO)_4$. The $NaCo(CO)_4$ dissolved in the water immediately. Then 85 mg of freshly metathesized [(bpy)Re^{I}(CO)$_3$(py)$^+$][Cl$^-$] (0.14 mmol) was placed into a Schlenk tube and dissolved in a mixture of 14 mL of distilled H_2O, 5 mL of CH_3OH, and 1 mL of CH_3CN. The resulting solution was degassed with argon. At this point, the room lights were turned off and the Schlenk tube containing the [(bpy)Re(CO)$_3$(py)$^+$][Cl$^-$] solution was covered with aluminum foil. Then the aqueous solution of $NaCo(CO)_4$ was slowly added via cannula to the Re(I) solution, whereupon complex **2a** was instantly apparent as a dark red precipitate. The mixture was stirred for 1 h, and then the solvents were removed under reduced pressure overnight. The product was washed two times with distilled H_2O in order to remove soluble salts. The purified product was obtained as a dark red solid; yield, 90 mg (100%).

(c) Crystallization of Complex 2a. Crystals of complex **2a** of sufficient quality for X-ray structure determination were obtained by the following procedure. First, 90 mg of complex **2a** was dissolved in approximately 1 mL of degassed CH_3CN. Then approximately 2 mL of dry (Na/K distilled), degassed Et_2O was carefully layered on top of the CH_3CN solution. The Schlenk tube was maintained under a positive pressure of argon, and after 2 days most of the solvent had evaporated, leaving complex **2a** as long, sharp, dark red needles. Repeated attempts to crystallize complexes **1a** and **3a** by the same procedure failed.

Spectral and Analytical Data. Complex 1a. ^{1}H NMR (300 MHz, CD_3CN): δ 4.10 (s, 6H, methyl), 7.27 (t, 2H, pyridine), 7.85 (t, 1H, pyridine), 8.20 (d, 2H, pyridine), 8.53 (d, 2H, dmeb), 8.73 (d, 2H, dmeb), 9.63 (s, 2H, dmeb). Low-resolution mass spectroscopy (FAB, positive ion, nitrobenzyl alcohol matrix). Calcd for $C_{22}H_{17}N_3O_7Re$ (M^+): 621.6. Found: 622.

Complex 2a. ^{1}H NMR (300 MHz, CD_3CN): δ 7.29 (t, 2H, pyridine), 7.79 (t, 1H, pyridine), 8.06 (t, 2H, pyridine), 8.26 (t, 2H, bpy), 8.39 (d, 2H, bpy), 8.60 (t, 2H, bpy), 9.21 (d, 2H, bpy). IR (KBr, cm^{-1}): 2026, 1937, 1923, 1880. Anal. Calcd for $C_{22}H_{13}N_3O_7ReCo$: C, 39.06; H, 1.94; N, 6.21; Found: C, 38.81; H, 1.99; N, 6.14.

Complex 3a. ^{1}H NMR (300 MHz, CD_3CN): δ 2.44 (s, 6H, methyl), 2.46 (s, 6H, methyl), 7.30 (t, 2H, pyridine), 7.86 (t, 1H, pyridine), 8.10 (s, 2H, tmb), 8.28 (d, 2H, pyridine), 8.87 (s, 2H, tmb). IR (KBr, cm^{-1}): 2032, 1948, 1922, 1877. Anal. Calcd for $C_{26}H_{21}N_3O_7ReCo$: C, 42.63; H, 2.89; N, 5.74; Found: C, 42.66; H, 3.02; N, 5.64.

Methods and Instrumentation for Physical Studies. Tetracarbonylcobaltate salts **1a**, **2a**, and **3a** were air-stable solids. However, the compounds decomposed rapidly in solution upon exposure to air and/or light. Thus, all solution preparations and serial dilutions were carried out in a nitrogen purged drybox (Vacuum Atmospheres). Absorption and fluorescence experiments were carried out with the samples contained in 1 × 1 cm cuvettes that were filled and then sealed inside the drybox using serum caps. Transient absorption studies were carried out with samples contained in a recirculating flow cell that contained 100 mL total volume to minimize the effects of sample decomposition during data acquisition.

Time resolved emission, steady state emission, transient absorption, UV−visible absorption, and electrochemistry were carried out using instrumentation that has been previously described.[87,88]

Dissociation Constants and Molar Absorptivity for Charge Transfer Salts. Dissociation constants for the contact ion pairs and molar absorptivities for the IPCT bands for complexes **1a**, **2a**, and **3a** were determined by the graphical method developed by Drago and Rose.[65] Briefly, the absorption at the charge transfer absorption maximum of THF solutions of complexes**1a**, **2a**, or **3a** was determined over the concentration range 0.1−7 mM. For each sample concentration a curve was constructed by plotting calculated values of K_d as a function of ϵ_{max} according to eq 13, where C is the concentration of the salt in

$$C^2\left(\frac{\epsilon_{max}}{A_{max}}\right) - 2C - \frac{A_{max}}{\epsilon_{max}} = K_d \qquad (13)$$

(83) Wang, Y.; Lucia, L. A.; Schanze, K. S. *J. Phys. Chem.* **1995**, *99*, 1961.
(84) Wang, Y.; Schanze, K. S. *J. Phys. Chem.* **1996**, *100*, 5408.
(85) MacQueen, D. B.; Schanze, K. S. *J. Am. Chem. Soc.* **1991**, *113*, 7470.
(86) Edgell, W. F.; Lyford, J., IV. *Inorg. Chem.* **1970**, *9*, 1932.
(87) Wang, Y.; Schanze, K. S. *Inorg. Chem.* **1994**, *33*, 1354.
(88) Wang, Y.; Schanze, K. S. *Chem. Phys.* **1993**, *176*, 305.

the solution, A_{max} is the absorptivity of the solution at the maximum of the IPCT absorption band, and ϵ_{max} is a "trial" set of molar absorptivity values. (For these studies plots were constructed by varying ϵ_{max} over the range 50−300 M^{-1} cm^{-1}). A family of curves was thus generated from the absorption measurements as a function of concentration. Then, the values of K_d and ϵ_{max} and estimated errors were obtained by visually determining the region where the plots intersected with highest density. In this manner it was possible to determine ϵ_{max} to within ±10% accuracy; however, the error in K_d was typically on the order of ±50%.

Transient Absorption Relative Actinometry Experiments. Quantum yields for formation of free radicals in the IPCT systems were determined by using transient absorption relative actinometry.[89] These studies were carried out on a nanosecond laser flash photolysis system that employed a Q-switched Nd:YAG laser for excitation. Experiments with 355 nm excitation were carried out as a function of laser energy over the range 0.2−5 mJ $pulse^{-1}$ (0.6−15 mJ cm^{-3} at the sample cell), while those with 532 nm excitation were carried out over the range 1−10 mJ $pulse^{-1}$ (3−30 mJ cm^{-3} at the sample cell). In every case the transient absorption signals due to excited states or reactive intermediates produced by the laser excitation were linear over this range.

For experiments carried out using near-UV laser excitation (355 nm) the ^{3}MLCT excited state of complex **2b** in CH_3CN solution was used as a transient absorption actinometer. The difference molar absorptivity of MLCT excited state **2b** at 370 nm was previously determined to be $\Delta\epsilon_{*Re}^{370nm} = 11\,900$ M^{-1} cm^{-1}.[47] Note that in using complex **2b** as an actinometer we implicitly assume that the ^{3}MLCT state is formed with unit quantum efficiency following 355 nm excitation. For experiments carried out using visible laser excitation (532 nm), the ^{3}MLCT state of $Ru(bpy)_3^{2+}$ in aqueous solution was used as the actinometer. The difference molar absorptivity of MLCT excited state $Ru(bpy)_3^{2+}$ at 370 nm ($\Delta\epsilon_{*Ru}^{370nm} = 12\,000$ M^{-1} cm^{-1}) was determined from the experimentally determined difference absorptivity at 370 and 450 nm (ΔA_{*Ru}^{370nm} and ΔA_{*Ru}^{450nm}, respectively) by the equation $\Delta\epsilon_{*Ru}^{370nm} = \Delta\epsilon_{*Ru}^{450nm}(\Delta A_{*Ru}^{370nm}/\Delta A_{*Ru}^{450nm})$, where $\Delta\epsilon_{*Ru}^{450nm} = -7600$ M^{-1} cm^{-1} was previously determined by Hoffman.[90]

Cage escape yields (Φ_{esc}) for formation of free radicals produced by 355 nm laser excitation of complexes **2a** and **3a** were determined as follows. A solution of complexes **2a** or **3a** was prepared with a concentration of 1.2×10^{-4} M (ground state absorbance at 355 nm, ca. 0.8 for 1 cm path length), and an actinometer solution of complex **2b** was prepared which had a matched ground state absorbance at 355 nm. Then the transient absorption of both solutions was determined as a function of laser power over the range 0.2−5 mJ/pulse. The cage escape yields were determined at each laser power according to eq 14,

$$\Phi_{esc} = \frac{1}{\eta_q}\frac{C_{Re^0}}{C_{*Re}} = \frac{(\Delta A_{Re^0}^{350nm}/\Delta\epsilon_{Re^0}^{350nm})}{(\Delta A_{*Re}^{370nm}/\Delta\epsilon_{*Re}^{370nm})} \quad (14)$$

where C_{*Re} is the initial concentration of MLCT excited state **2b** produced by laser excitation of the actinometer solution; C_{Re^0} is the concentration of the reduced complex $(b^{\bullet-})Re^I(CO)_3(py)$, formed in the sample solution of complex **2a** or **3a**; η_q is the fraction of MLCT excited states that is quenched by $Co(CO)_4^-$ ($\eta_q \approx 1$ under the conditions of the experiments); $\Delta A_{Re^0}^{350nm}$ is the difference absorptivity at 350 nm in the sample solution; $\Delta\epsilon_{Re^0}^{350nm}$ is the difference molar absorptivity at 350 nm for the reduced complex, $(b^{\bullet-})Re^I(CO)_3(py)$ (6500 M^{-1} cm^{-1} for diimine = bpy and 7000 M^{-1} cm^{-1} for diimine = tmb);[91] ΔA_{*Re}^{370nm} is the difference absorptivity at 370 nm immediately following the laser pulse in the complex **2b** actinometer solution; and $\Delta\epsilon_{*Re}^{370nm} = 11\,900$ M^{-1} cm^{-1} as described above. Generally, Φ_{esc} varied by less than ± 5% over the range of laser powers used.

Cage escape yields (Φ_{esc}) for formation of free radicals produced by 532 nm laser excitation of complexes **2a** and **3a** were determined as follows. A solution of complex **2a** or **3a** was prepared with a concentration of 1.2×10^{-3} M (ground state absorbance at 532 nm, ca. 0.2 for 1 cm path length), and an actinometer solution of $Ru(bpy)_3^{2+}$ in H_2O was prepared which had a matched ground state absorbance at 532 nm. Then the transient absorption of both solutions was determined as a function of laser power over the range 1−10 mJ/pulse. The cage escape yields were determined at each laser power according to eq 15,

$$\Phi_{esc} = \frac{C_{Re^0}}{C_{*Ru}} = \frac{(\Delta A_{Re^0}^{490nm}/\Delta\epsilon_{Re^0}^{490nm})}{(\Delta A_{*Ru}^{370nm}/\Delta\epsilon_{*Ru}^{370nm})} \quad (15)$$

where C_{*Ru} is the initial concentration of MLCT excited state $Ru(bpy)_3^{2+}$ produced by laser excitation of the actinometer solution; C_{Re^0} is the concentration of the reduced complex $(b^{\bullet-})Re^I(CO)_3(py)$, formed in the sample solution of complex **2a** or **3a**; $\Delta A_{Re^0}^{490nm}$ is the difference absorptivity at 490 nm in the sample solution; $\Delta\epsilon_{Re^0}^{490nm}$ is the difference molar absorptivity at 490 nm for the reduced complex, $(b^{\bullet-})Re^I(CO)_3(py)$ (3700 M^{-1} cm^{-1} for b = bpy and tmb); ΔA_{*Ru}^{370nm} is the difference absorptivity at 370 nm immediately following laser excitation in the $Ru(bpy)_3^{2+}$ actinometer solution; and $\Delta\epsilon_{*Ru}^{370nm} = 12\,000$ M^{-1} cm^{-1} as described above. Generally, Φ_{esc} varied by less than ±10% over the range of laser powers used.

Crystal Structure Determination. Data were collected at room temperature on a Siemens R3m/V diffractometer equipped with a graphite monochromator utilizing Mo K_α radiation ($\lambda = 0.710\,73$ Å). A set of 40 reflections with $20.0° \le 2\theta \le 22.0°$ was used to refine the cell parameters; 9185 reflections were collected using the ω-scan method. Four reflections were measured every 96 reflections to monitor instrument and crystal stability (maximum correction on I was <2%). Absorption corrections were applied on the basis of measured crystal faces using SHELXTL plus[92] (absorption coefficient, $\mu = 5.83$ mm^{-1}(minimum and maximum transmission factors are 0.395 and 0.568, respectively)).

The structure was solved by the heavy atom method in SHELXTL plus from which the locations of the Re and Co atoms were obtained. The rest of the non-hydrogen atoms were obtained from a subsequent difference Fourier map. The structure was refined in SHELXTL plus using full-matrix least squares. The non-H atoms were treated anisotropically, whereas the positions of the hydrogen atoms were calculated in ideal positions and their isotropic thermal parameters were fixed. A set of 613 parameters was refined, and $\sum w(|F_o| - |F_c|)^2$ was minimized; $w = 1/(\sigma|F_o|)^2$, $\sigma(F_o) = 0.5\ kI^{-1/2}\{[\sigma(I)]^2 + (0.02I)^2\}^{1/2}$, I(intensity) = $(I_{peak} - I_{background})$(scan rate), $\sigma(I) = (I_{peak} + I_{background})^{1/2}$ (scan rate), k is the correction due to decay and Lorentz polarization effects, 0.02 is a factor used to down weight intense reflections and to account for instrument instability. The linear absorption coefficient was calculated from values from the *International Tables for X-ray Crystallography*.[93] Scattering factors for non-hydrogen atoms were taken from Cromer and Mann[94] with anomalous-dispersion corrections from Cromer and Liberman,[95] while those of hydrogen atoms were from Stewart, Davidson, and Simpson.[96]

Acknowledgment. We gratefully acknowledge the National Science Foundation for support of this work (Grant No. CHE-9401620).

Supporting Information Available: Supplementary Tables 1−5 listing fractional coordinates, bond lengths and angles, and anisotropic thermal parameters and one figure showing a crystal packing diagram (10 pages). Ordering information is given on any current masthead page.

IC970351N

(89) Carmichael, I.; Hug, G. L. *J. Phys. Chem. Ref. Data* **1986**, *15*, 1.
(90) Hoffman, M. Z. *J. Phys. Chem.* **1988**, *92*, 3458.
(91) Lucia, L. A. Ph.D. Dissertation, University of Florida, 1996.
(92) Sheldrick, G. M. *SHELXTL plus*; Nicolet XRD Corp.: Madison, WI, 1990.
(93) *International Tables for X-ray Crystallography*; Kynoch Press: Birmingham, England, 1974; Vol. IV, p 55 (present distributor: Reidel: Dordrecht, The Netherlands).
(94) Cromer, D. T.; Mann, J. B. *Acta Crystallogr.* **1968**, *A24*, 321.
(95) Cromer, D. T.; Liberman, D. *J. Chem. Phys.* **1970**, *53*, 1891.
(96) Stewart, R. F.; Davidson, E. R.; Simpson, W. T. *J. Chem. Phys.* **1965**, *42*, 3175.